Electronic Supplementary Information

Resonator-based add-drop filters enabled by flexible polymorphic crystals with TADF-RTP motifs

Pradip Pattanayak,[a‡] Ankur Khapre, [b‡] Shamim Ahmad,[a] Avulu Vinod Kumar,[b] Bishes Ray,[a] Satendra Kumar,[a] Chilla Malla Reddy,[c] Rajadurai Chandrasekar [b] and Pradipta Purkayastha[a]**

[a]Department of Chemical Sciences and Center for Advanced Functional Materials, Indian Institute of Science Education and Research, Kolkata, Mohanpur 741246, West Bengal, India

[b]Advanced Photonic Materials and Technology Laboratory, School of Chemistry and Centre for Nanotechnology, University of Hyderabad, Prof. C. R. Rao Road, Gachibowli, Hyderabad 500046, Telangana, India

[c]Department of Chemistry, Indian Institute of Technology Hyderabad, Hyderabad, 502285, Telangana, India

---

‡ Equal contribution of authors

Table of Contents:

1. Materials

All materials were used without any prior purification. 9-Ethylcarbazole-3-boronic acid, 5-Bromo-2,2`-bithiophene-5`-carboxaldehyde, Tetrakis(triphenylphosphine) palladium(0) were purchased from TCI Chemicals. Potassium carbonate was purchased from Merck. Spectroscopic grade solvents from Merck were used for synthesis and other experiments.

2. Instrumental Methods

a) NMR spectroscopy: ^{1}H and ^{13}C NMR spectra were recorded on a Bruker DPX spectrometer 500 MHz spectrometer with a solvent proton as internal standard (DMSO-d_6: ^{1}H: 2.47 ppm; $CDCl_3$: ^{13}C: 77.16 ppm). Commercially available deuterated $CDCl_3$ and DMSO-d_6 was used. Chemical shifts (δ) are given in parts per million (ppm). Spectra were processed using topspin 4.3.0 software.

b) Optical studies: The UV-VIS spectroscopy was done in a U2900 spectrophotometer from HITACHI using a quartz cuvette (path length of 1 cm) for solutions and 1 cm × 1 cm quartz plate for film state. Steady-state and time resolved PL measurement were performed in a QuantaMaster 40 machine from PTI (Xe-lamp), time-correlated single-photon counting (TCSPC) methods with HORIBA JOBIN S3 YVON (single photon counting controller: Fluorohub, precision photo multiplayer power supply: Fluoro3PS), and FLS 1000 Photoluminescence Spectrometer (Xe-400 lamp, µF-400-microsecond flashlamp, PMT-900 detector) from Edinburgh Instruments. PL spectra of solid-state (film/crystal) were recorded in a front-face geometry. Temperature-dependent PL experiment in solid-state is performed in FLS1000 with the cryostat (Oxford Instruments Optistat DN model) setup using liquid nitrogen as a cryogen. Absolute quantum yields were measured using an integrating sphere (using Xe-400 lamp and PMT-900 + Integrating sphere detector). The singlet-triplet energy gap was estimated from the onset of the fluorescence and phosphorescence spectra for both polymorphs.

Briefly, fluorescence spectra were recorded at room temperature, where the emission is attributed to the singlet excited state. Phosphorescence spectra were then recorded at 78 K using a 10 ms delay to eliminate any residual singlet contribution. The onsets of the normalized fluorescence (singlet) and phosphorescence (triplet) spectra were used to experimentally determine the singlet-triplet energy gap.

c) Single crystal X-ray diffraction: Single crystal X-ray diffraction (SCXRD): SCXRD data was collected at 279 K for the macro crystal on a Rigaku (dual, Cu/Mo at zero Eos) diffractometer using monochromatic Cu-K_α radiation having a 100 μm beam size. The structure was solved by Olex2 (1.2.9 version) with the SHELXT structure solution program via intrinsic phasing algorithm and the ShelXL refinement package using Least Squares minimization was utilized to refine the structure.1-2 Displacement parameters of all non-hydrogen atoms were refined anisotropically. Mercury (4.2.0 version) software was used to prepare all the crystal packing diagrams.

d) Confocal Microspectroscopy studies: The optical experiments of a single microcrystal were carried out on a backscattering mode setup of the Wi-Tec alpha 300 AR laser confocal optical microscope (LCOM) equipped with a Peltier-cooled CCD detector. Using 300 grooves/mm grating BLZ = 750 nm, the accumulation time was adjusted to 30 s and the integration time was typically made 0.5 s. Ten averaged accumulations obtain each single spectrum. A diode 405 nm laser source was used for optical excitation of the polymorphic crystal waveguides via a 60× objective. Unless otherwise specified, a 20× objectives were used for spectra and image collection. All the experiments were carried out under ambient conditions.

e) Micromanipulation of the crystals: The micromanipulation experiments were performed using an AFM facility attached to the above-mentioned confocal microscope setup. Single microcrystals of G and Y polymorphic crystal waveguides were studied separately. Then the

OR polymorphic crystal waveguide was transferred onto the coverslip (borosilicate; Borosil), containing GY crystals, using AFM cantilever. An AFM cantilever (TipsNano: NSG10, force constant 3.1 − 37.6 N/m) was used for the mechanical manipulation. For a typical bending/micromechanical manipulation experiment, the AFM-tip was held constant at a height above the piezo stage containing microcrystals, and the piezo stage was carefully manoeuvred in ±x and ±y directions to bring mechanical deformation in the microcrystal.

f) Nanoindentation: Nanoindentation experiments have been performed on the side and top faces of single crystals using the TI Premier from Hysitron, Minneapolis, USA, equipped with an in-situ Scanning Probe Microscope (SPM). A Berkovich tip (three-sided pyramidal tip with a total included plane-edge angle of 142.3°) of radius ~150 nm was used to determine the hardness (H) and elastic modulus (E) of the crystals. The H and E were extracted using the standard Oliver Pharr (O&P) method (12).

g) Field-Emission Scanning Electron Microscopy: The morphological analysis was performed using a Zeiss field-emission scanning electron microscope (FESEM) operating at 5 keV. All the experiments were performed after gold coating the samples prior to imaging.

h) Transmission Electron Microscopy (TEM): Transmission Electron Microscopy (TEM) images and Single Atom Electron Diffraction (SAED) pattern of different samples were recorded on a JEOL, JEM-2100F microscope using a 200 kV electron source at the DST-FIST facility in IISER Kolkata. Samples were prepared on a Cu grid (Carbon Type-B, 300 mesh, TED PELLA) by drop casting technique and evaporating the sample under air.

i) Atomic force microscopy (AFM): Atomic force microscopy (AFM) was performed using Cypher Asylum Research AFM, Oxford Instruments. Post-processing of the AFM data was done using the interfaced software.

3. Synthesis of CZ-CHO: 1 g (4.18 mmol) of 9-Ethylcarbazole-3-boronic acid, 1.14 g (4.18 mmol) of 5-Bromo-2,2`-bithiophene-5`-carboxaldehyde and 0.69 g (5 mmol) potassium carbonate were added to a mixture of 10 mL Toluene, 2 mL Ethanol and 1 mL water in a pressure tube. The mixture was vigorously purged with nitrogen and stirred at room temperature. Finally, 210 mg (5 mol%) Tetrakis(triphenylphosphine)palladium (0) was added, and the pressure tube was sealed and heated overnight (12 hrs) at 110°C. After completion of the reaction, the solvents were first evaporated, and the mixture was worked up with ethyl acetate and water. Finally, silica gel column chromatography (n-hexane and ethyl acetate) gave the product a yellow crystalline solid (1.21 g,Yield ≈75%). δ (**^{1}H NMR** DMSO-d_6): 9.8 (s, 1H), 8.52 (d, 1H), 7.99 (d, 1H), 7.79, (d, 1H), 7.67 (d, 2H), 7.6 (m, 2H), 7.53 (t, 1H), 7.46 (t, 1H), 7.21 (t, 1H), 4.45 (m, 2H), 1.21 (m, 3H) ; δ (**^{13}C NMR** $CDCl_3$): 182.44, 147.75, 146.29, 141.27, 140.50, 137.55, 133.77, 133.22, 129.41, 127.34, 126.63, 124.83, 124.64 123.14, 123.05, 122.79, 120.64, 119.34, 117.94, 108.94, 108.80, 37.74, 13.86.

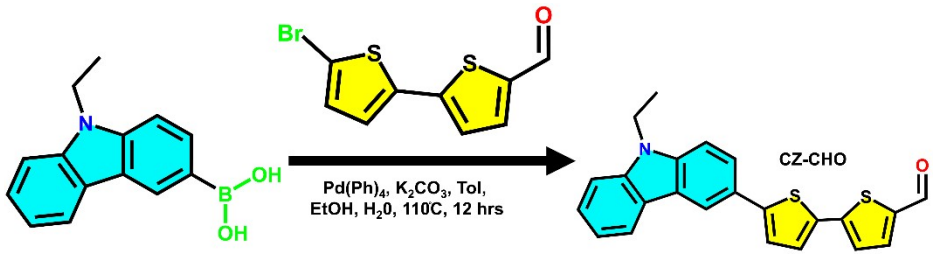

Scheme S1. Synthetic route for the preparation of CZ-CHO.

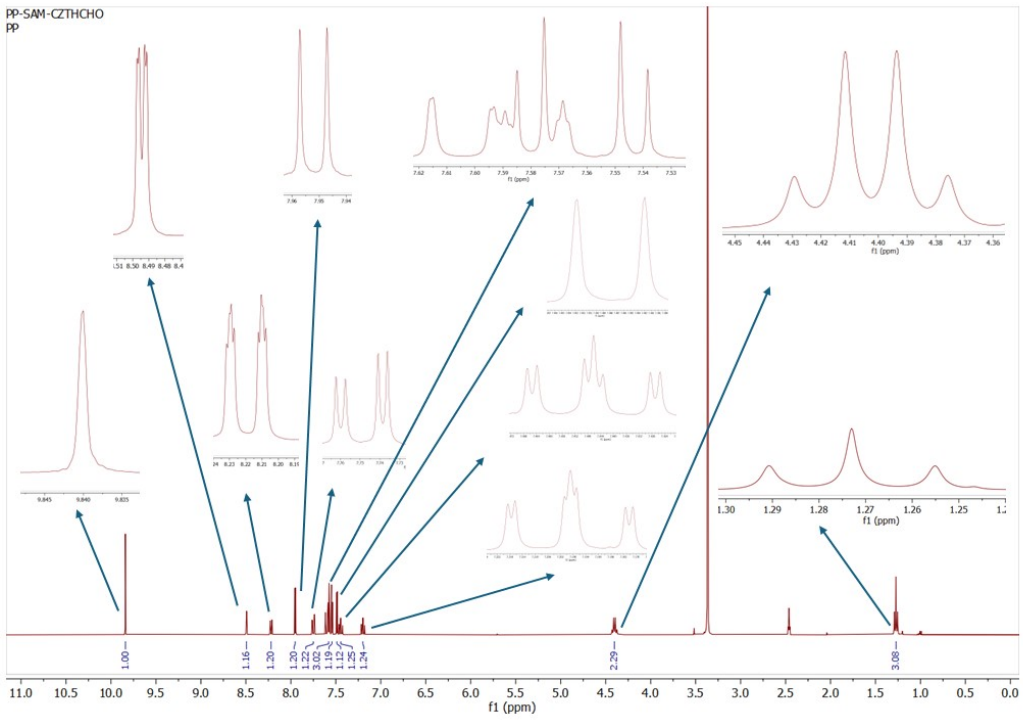

Fig. S1. ^{1}H NMR spectrum of CZ-CHO in DMSO-d_6.

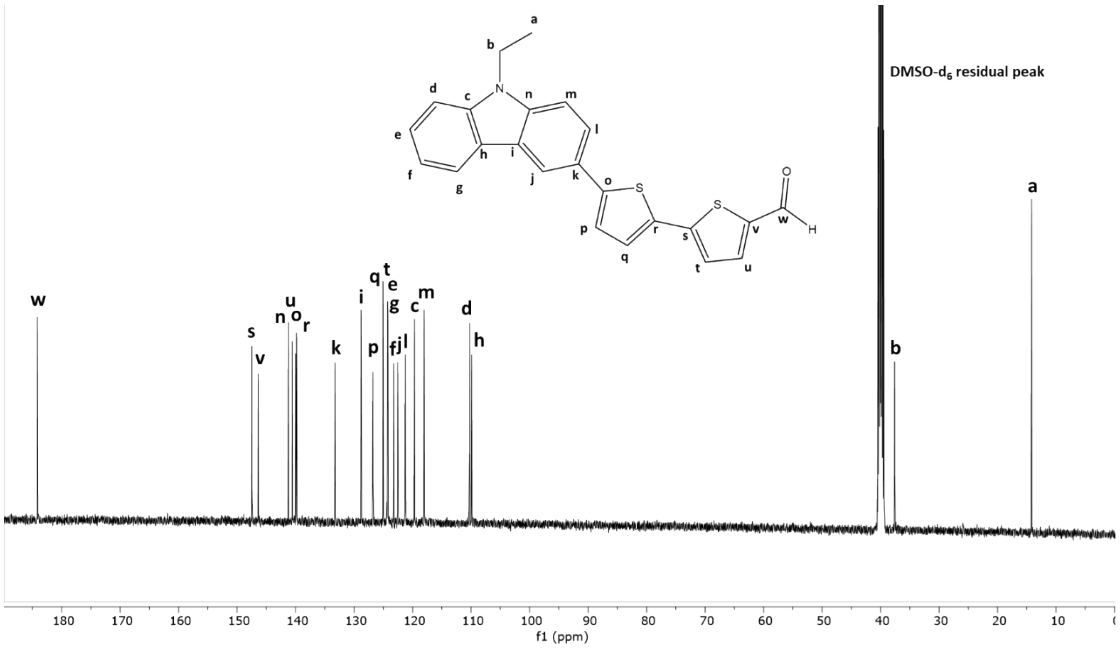

Fig. S2. ^{13}C NMR spectrum of CZ-CHO in DMSO.

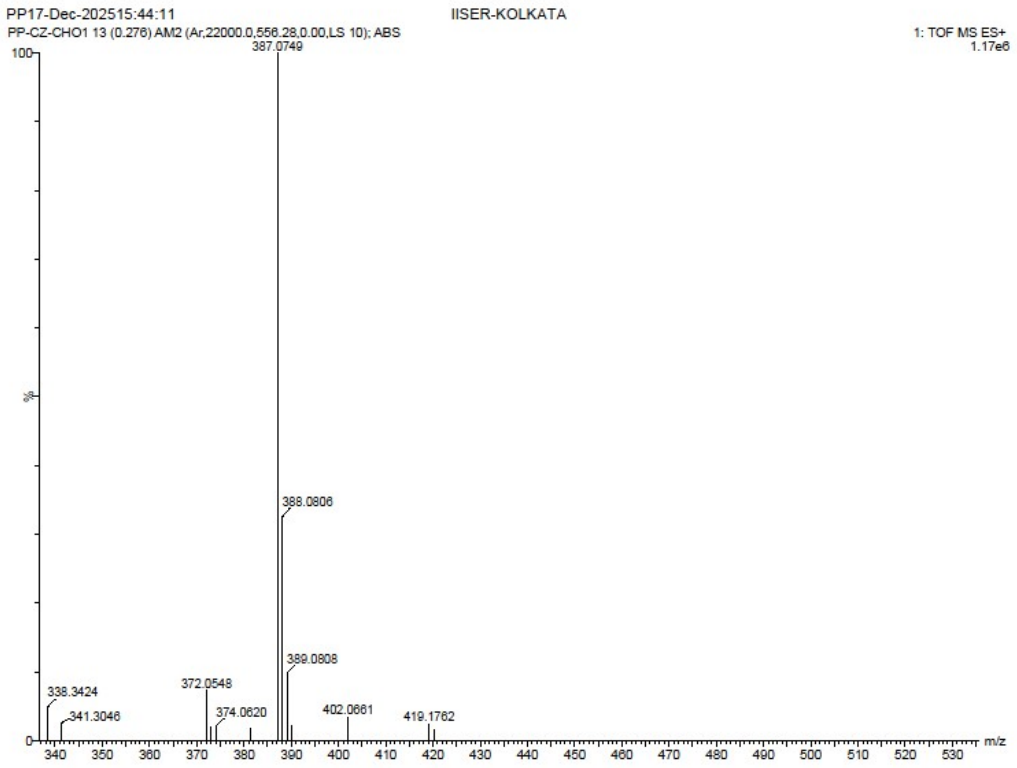

Fig. S3. HRMS of CZ-CHO.

4. X-ray Diffraction Studies of CZ-CHO

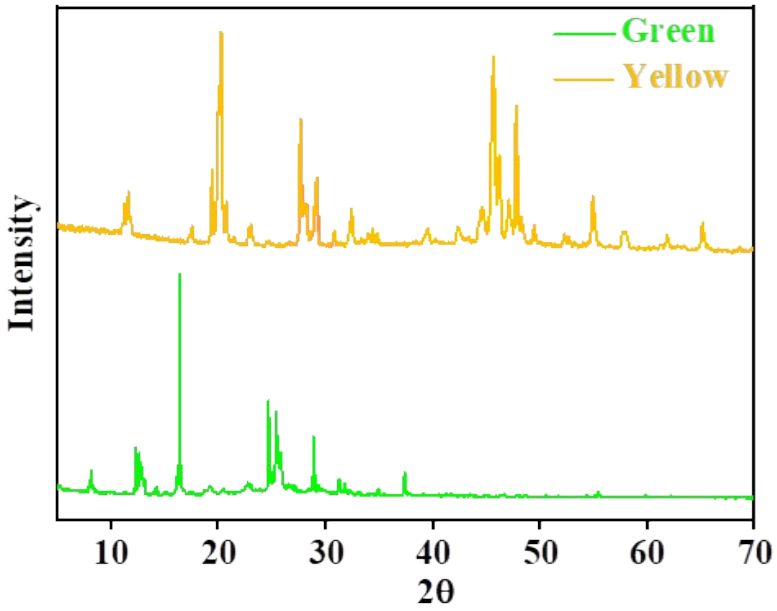

Fig. S4. PXRD patterns of CZ-CHO polymorphs.

Single crystal XRD studies of CZ-CHO polymorphs

Table S1. SCXRD Data

	Green Crystal	Yellow Crystal
CCDC #	2484035	2484038
Space group	P -1	P -1
Crystal system	Triclinic	Triclinic
a, b, c	a = 23.87 Å, b = 6.56 Å, c = 13.42 Å	a = 10.29 Å, b = 17.72 Å, c = 25.03 Å
α, β, γ	α = 90.00°, β = 97.86°, γ = 90.00°	α = 94.28°, β = 93.14°, γ = 90.41°
Volume	2083.71	4546.47

5. Solid-state optical studies of G and Y polymorphs

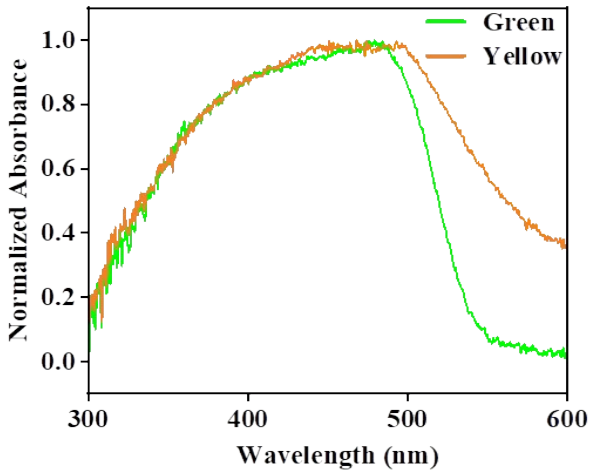

Fig. S5. Absorption spectra of CZ-CHO polymorphs.

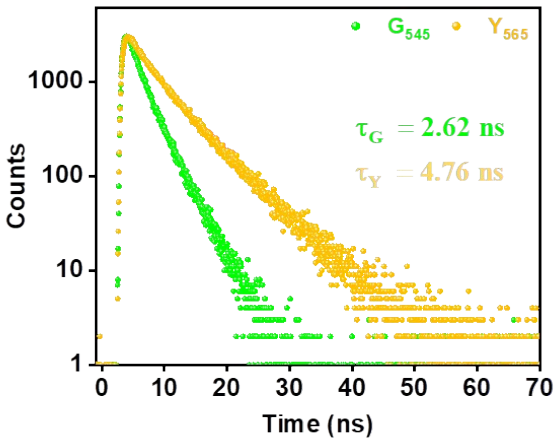

Fig. S6. Prompt PL decay patterns of CZ-CHO polymorphs at room temperature.

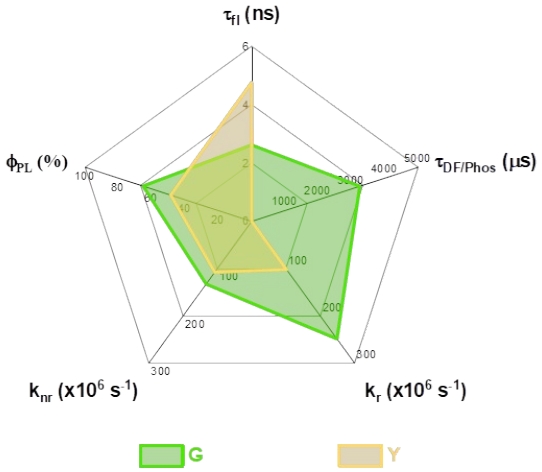

Fig. S7. Radar plot of photophysical parameters for CZ-CHO polymorphs.

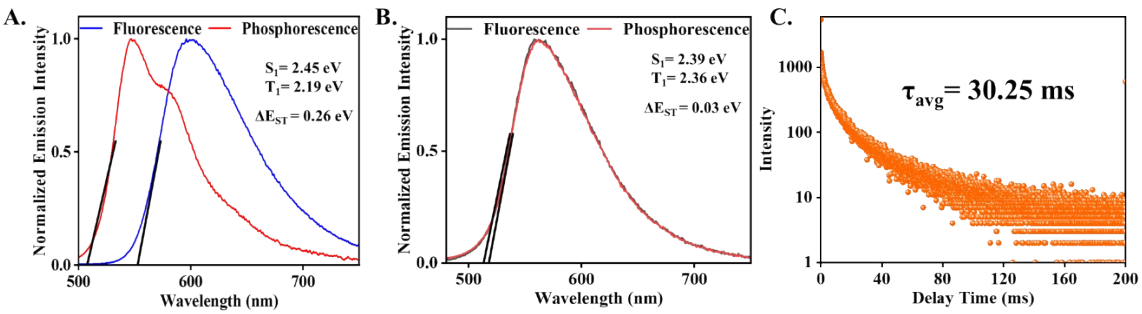

Fig. S8. Fluorescence and phosphorescence (20 ms delay, 78 K) spectra and their corresponding singlet-triplet energy of G (A) and Y (B) crystals respectively and (C) phosphorescent lifetime of Y crystals measured at 78 K.

Table S2. Photophysical parameters of the CZ-CHO polymorphs. (**a**: measurement under ambient conditions; **b**: measured at 78 K).

Polymorph	$\lambda_{abs}{}^{a}$ (nm)	$\lambda_{Fl}{}^{a}$ (nm)	$\lambda_{Ph}{}^{a}$ (nm)	ΔE_{S-T} (eV)	$\tau_{Fl}{}^{a}$ (ns)	$\tau_{DF}{}^{a}$ (μs)	$\tau_{DF}{}^{b}$ (μs)	$\tau_{Ph}{}^{a}$ (ms)	$\tau_{Ph}{}^{b}$ (ms)	Φ_{PL} (%)
G	504	545	600	0.26	2.62			3.25	7.98	65.2
Y	517	565		0.003	4.46	5.75	2.68		30.25	48.7

6. Mechanical Properties of G and Y polymorphs

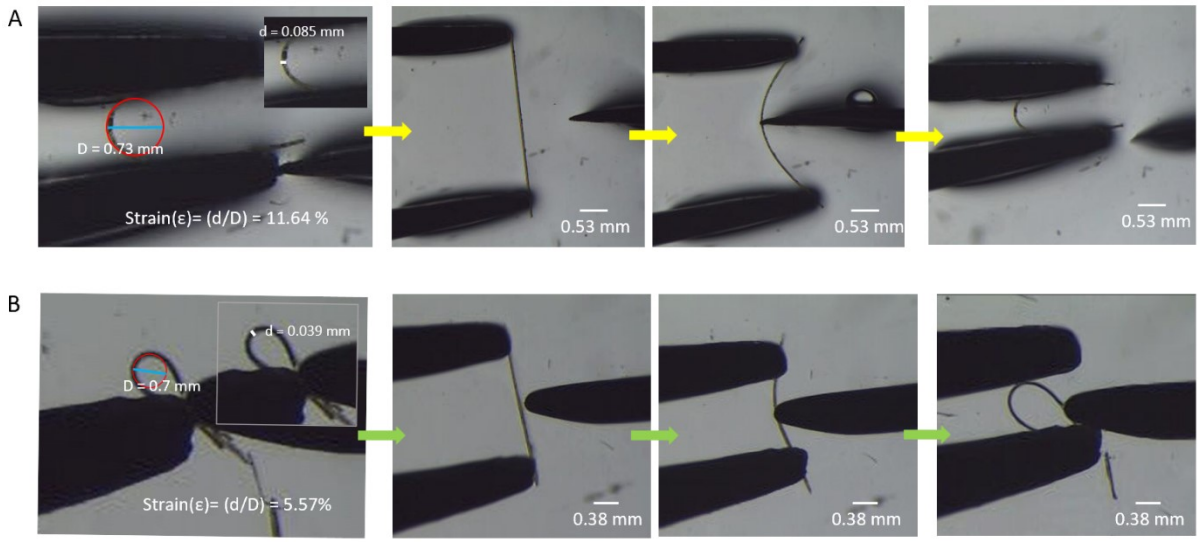

Fig. S9. Calculation of elastic strain for the green and yellow form with maximum bending represented in A and B respectively. D = diameter of the circles and d = thickness of the crystals in mm, ε = % elastic strain.

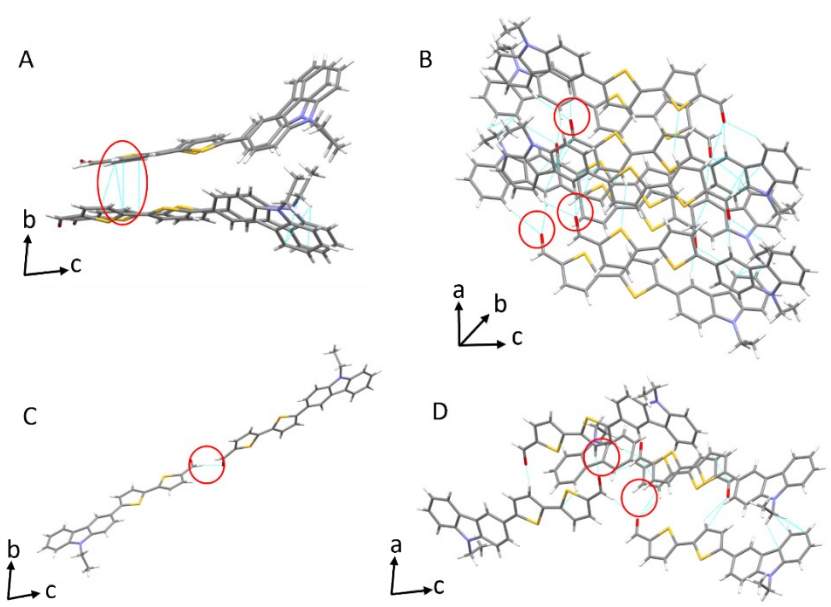

Fig. S10. (A, B) Depicting assymetric unit with π-π interaction and bifurcated C–H···O hydrogen bonding in green form , (C, D) representing assymetric unit with C–H···O hydrogen bonding between molecules and bifurcated C–H···O hydrogen bonding with different molecules in yellow form.

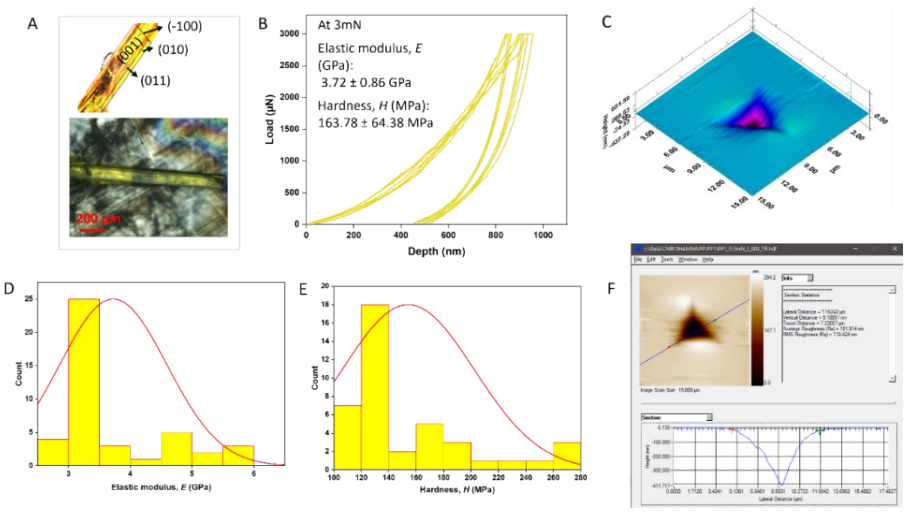

Fig. S11. Mechanical characterization from the nanoindentation experiment of green polymorph; (A) image of the indented crystal (indexed faces in the inset), (B) multiple *P*–*h* curves with the *E*, *H* values at 3mN, (C) 3D impression, (D, E) are the histogram plots for the modulus and hardness, (F) height profile diagram after SPM imaging.

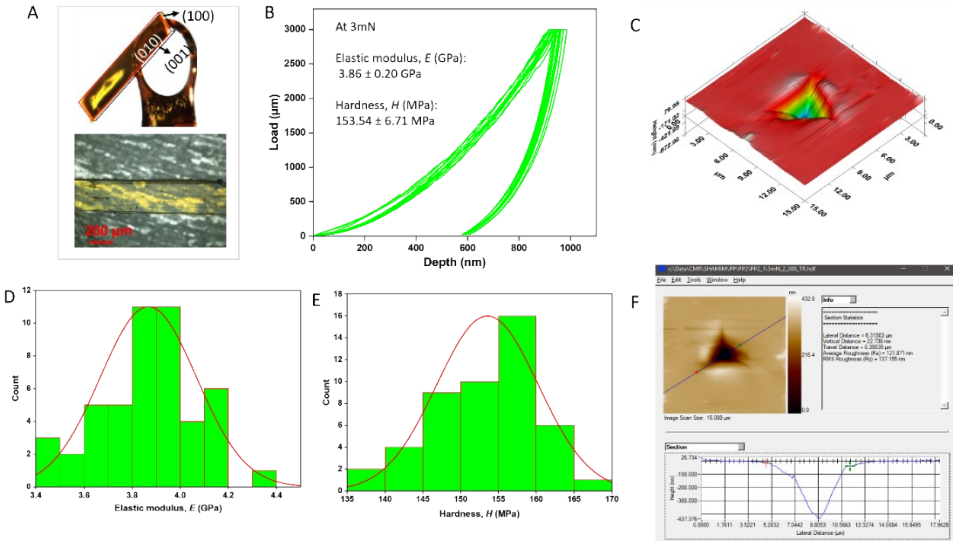

Fig. S12. Mechanical characterization from the nanoindentation experiment of yellow polymorph; (A) image of the indented crystal (indexed faces of a crystal in the inset). (B) multiple $P - h$ curves with the E, H values at 3mN load. (C) 3D impression image, (D, E) are the histogram plots for the modulus and hardness. (F) height profile diagram after SPM imaging.

Table S3. Tabulated values of the different parameters extracted from the nanoindentation studies for the green and yellow polymorph at 3 mN, 5 mN loads.

Polymorphs	Elastic modulus (GPa)		Hardness (MPa)		Contact depth (nm)	
	3 nm	5 nm	3 nm	5 nm	3 nm	5 nm
G	3.72 ± 0.86	3.38 ± 0.13	163.78 ± 64.38	130.74 ± 10.12	868.90 ± 131.97	1212.95 ± 46.16
Y	3.86 ± 0.20	3.63 ± 0.17	153.54 ± 6.71	146.98 ± 8.73	861.05 ± 19.37	1142.03 ± 34.46

7. Optical Waveguide and polymorphic add-drop filter (P-ADF) photonic circuit from G and Y polymorphs

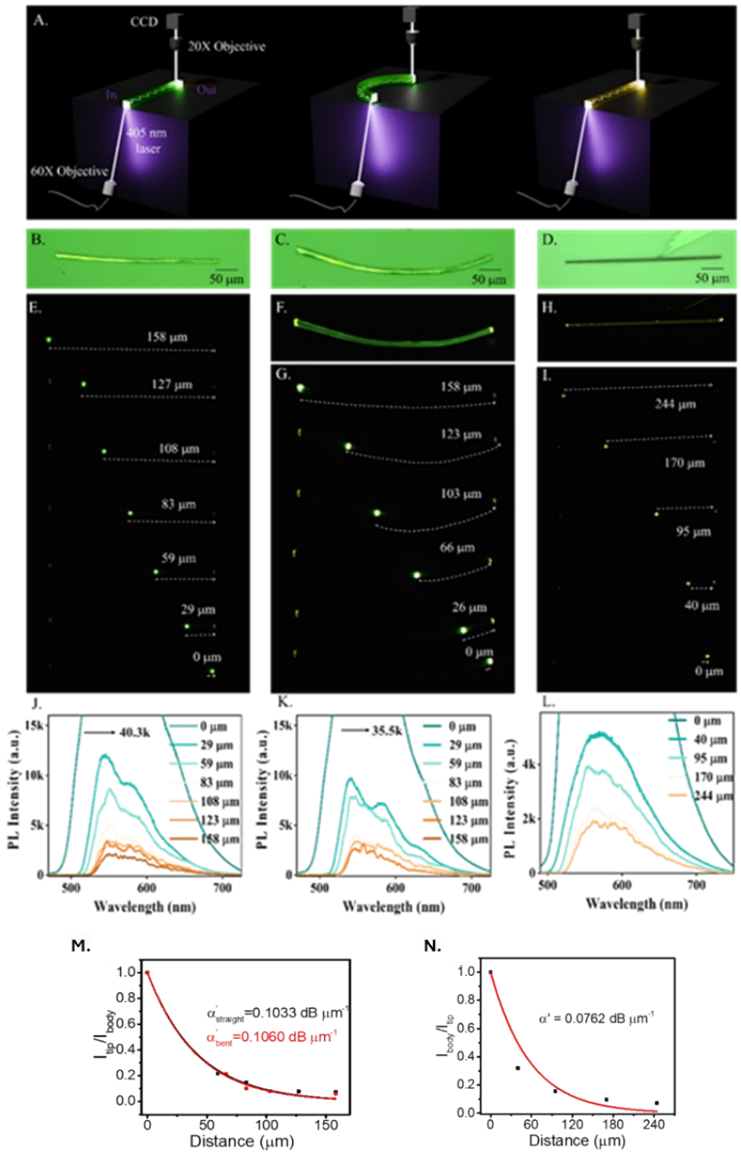

Fig. S13. (A) A schematic representation of the optical waveguide measurement experimental setup; (B-D) confocal optical; (F and H) FL microscope images of mechanically bent and straight G and Y crystal waveguides of CZ-CHO; (E, G and I) optical waveguides of straight green crystal, bent green crystal, and straight yellow crystal, respectively; (J-L) FL spectra for multiple optical path lengths in straight G, bent G, and straight Y crystal waveguides collected at the right end; (M and N) optical loss coefficient calculated from the fit of I_{tip}/I_{body} vs. distance for G and Y CZ-CHO microcrystals, respectively.

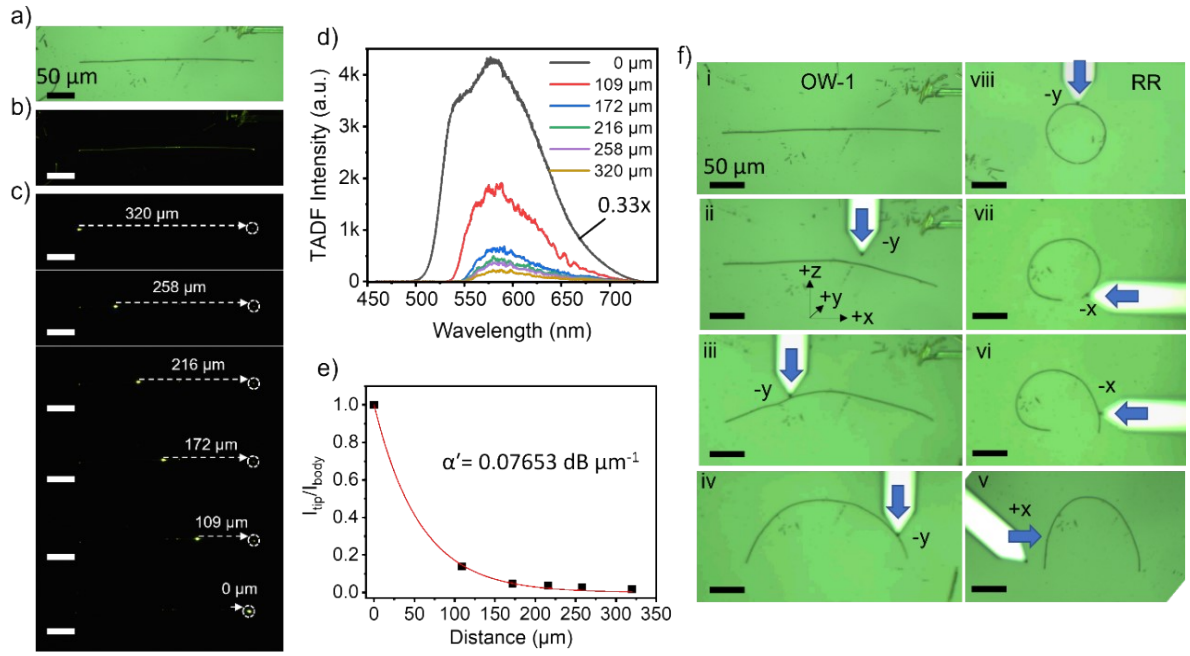

Fig. S14. (a) Confocal microscopy bright field, and (b) FL images of OW1 (Y-polymorph of CZ-CHO). (c) Dark field images for position-dependent excitation experiment with 405 nm laser (power 1.7 µW) on OW1, and (d) its corresponding optical spectra. (e) Optical loss coefficient estimation by nonlinear fitting (red line) the plot of I_{tip}/I_{body} VS signal propagation distance. (f) Sequential optical microscopy images demonstrating the steps involved in the mechanical micromanipulation of straight OW1 microcrystal into closed ring geometry using AFM cantilever tip (scale bar: 50 µm).

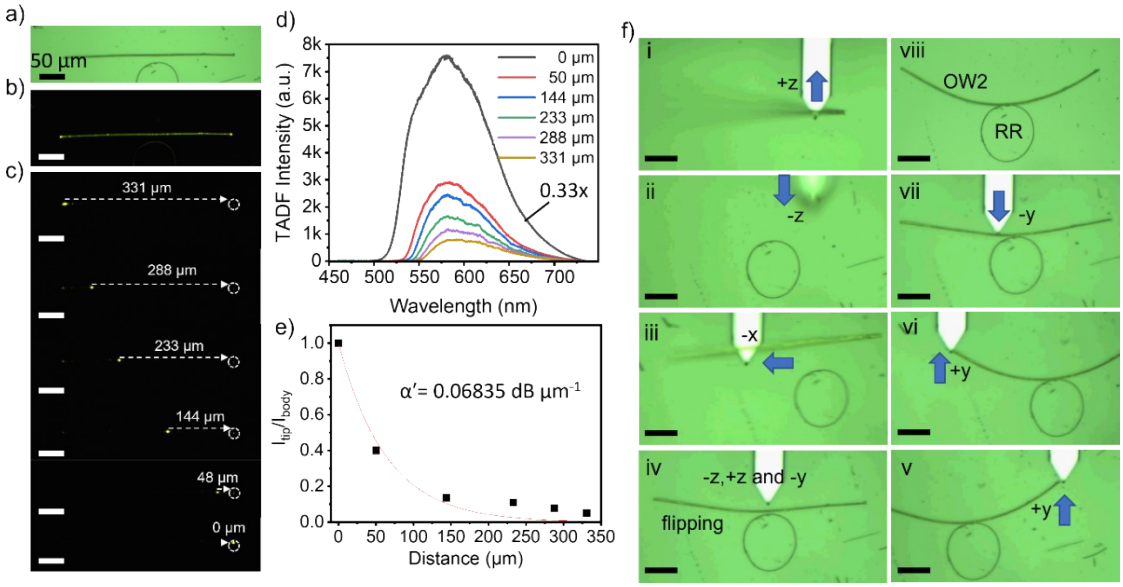

Fig. S15. (a) Confocal microscopy bright field, and (b) FL images of OW2 (Y-polymorph of CZ-CHO). (c) Dark field images for position dependent excitation experiment with 405 nm laser (power 1.7 µW) on OW2, and (d) its corresponding optical spectra. (e) Optical loss coefficient estimation by nonlinear fitting (red line) the plot of I_{tip}/I_{body} VS signal propagation distance. (f) Sequential optical microscopy images demonstrating the steps involved into the mechanical micromanipulation for straight OW2 microcrystal to approach towards the ring resonator to produce arc geometry attaching the middle part of OW2 to RR using AFM cantilever tip (scale bar: 50 µm).

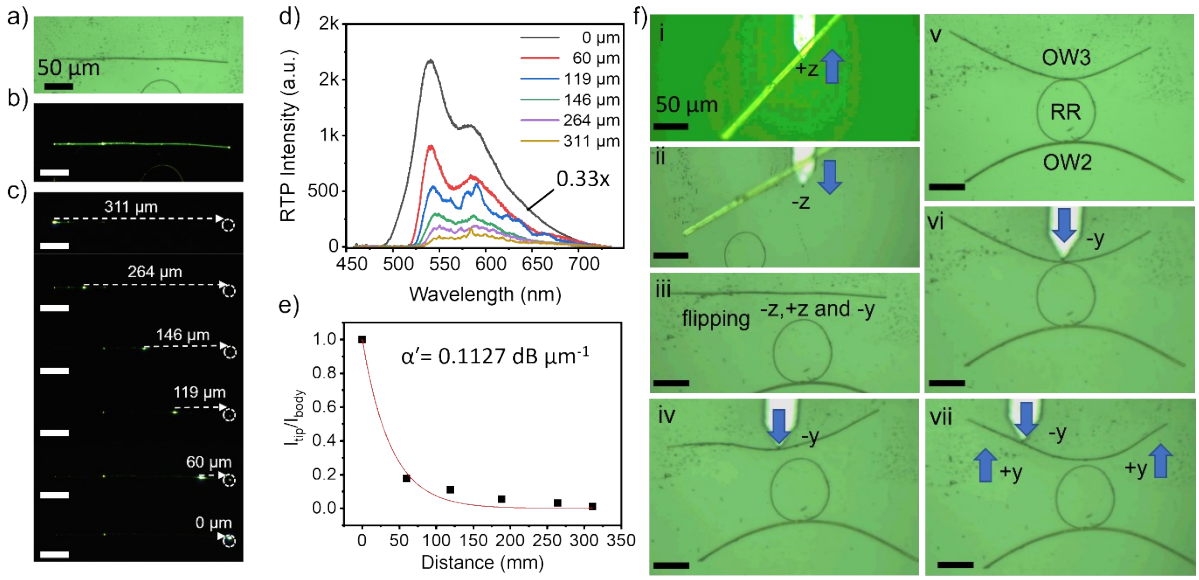

Fig. S16. (a) Confocal microscopy bright field, and (b) FL images of OW3 (GY polymorph of CZ-CHO). (c) Dark field images for position-dependent excitation experiment with 405 nm laser (power 1.7 µW) on OW3, and (d) its corresponding optical spectra. (e) Optical loss coefficient estimation by nonlinear fitting the plot of I_{tip}/I_{body} VS signal propagation distance. (f) Sequential optical microscopy images demonstrating the steps involved in the mechanical micromanipulation of a straight OW3 microcrystal towards the ADF construction using an AFM cantilever tip (scale bar: 50 µm).